

1 **Sensory convergence in the world’s largest cavefish diversification: patterns of**
2 **neuromast evolution, distribution and associated behaviour in *Sinocyclocheilus***

3

4 Bing Chen¹, Tingru Mao¹, Yewei Liu¹, Wenzhang Dai¹, Xianglin Li¹, Jian Yang², Joshua
5 B. Gross³, Madhava Meegaskumbura^{1*}

6

7 ¹ Guangxi Key Laboratory for Forest Ecology and Conservation, College of Forestry,
8 Guangxi University, Nanning, Guangxi, China

9 ² Key Laboratory of Environment Change and Resource Use, Beibu Gulf, Nanning
10 Normal University, Nanning, Guangxi, China

11 ³ Department of Biological Sciences, University of Cincinnati, Cincinnati, OH 45221,
12 U.S.A.

13

14

15 Corresponding author *E-mail* : madhava_m@mac.com

16 **Abstract**

17 *Sinocyclocheilus* represents the largest freshwater cavefish genus in the world. This
18 emerging model system is endemic to the southern Chinese karstic landscape, and
19 demonstrates multiple adaptations for life in caves (troglomorphy), with eye-
20 degeneration being the most pronounced. The less-apparent lateral line system, which
21 is often expanded in cave-dwellers, has been studied in other cavefish systems, but
22 never in the context of this diversification. Here we investigated the distribution and
23 evolution of cephalic neuromasts in 26 *Sinocyclocheilus* species. We used live-staining
24 and behavioural assays, and interpreted results in a phylogenetic context. We show that
25 asymmetry in neuromast features and the rate of evolution is greater in cave-adapted
26 species. Ancestral state reconstructions show that most *Sinocyclocheilus* are right-
27 biased with some scatter, and show convergence of neuromast phenotypes. There is
28 substantial variation in cephalic neuromast distribution patterns between and (to a lesser
29 extent) within species. Behavioural assays show blind species have a distinctive wall-
30 following behaviour. We explain these patterns in the context of the deep evolutionary
31 history associated with this karstic region, other traits, and habitat occupation of these
32 remarkable diversifications of fishes. Interestingly, some of these neuromast patterns
33 and behaviour show convergence with other phylogenetically distant cavefish systems.

34

35 **Key words:** Asymmetry, convergence, ancestral state reconstructions, wall-following
36 behaviour, live staining, troglomorphy

37 **Background**

38 Cave-dwelling (hypogean) fish provide a valuable system to study evolutionary novelty
39 [1-4], owing to the extreme conditions associated with these habitats, such as limited
40 food and perpetual darkness. Strong selective pressures arising from this extreme
41 environment are associated with a suite of morphological changes, such as eye
42 regression [5, 6]. However, numerous constructive features also evolve in cave-
43 dwellers. Among the most notable are expansions of the mechanosensory lateral line
44 system [7]. Here, we examine the nature of these expansions in the context of the
45 species-rich genus *Sinocyclocheilus*, an emerging model system and the largest
46 diversification of freshwater cavefish in the world [8, 9].

47 Neuromast organs are composed of hair cells with cilia embedded in a gelatinous
48 cupula, surrounded by a complex set of support cells [10, 11]. There are two general
49 neuromast types: canal neuromasts (CN), which are larger, and embedded in a bony
50 canal, and superficial neuromasts (SN), which project directly from the skin epithelium
51 [12-14]. In the Mexican tetra (*Astyanax*), cave morphs harbor variation in the number
52 and size of both types of neuromasts, including several-fold more SNs compared to
53 surface fish. Moreover, *Astyanax* cave morphs have a highly asymmetric distribution
54 of neuromasts across left/right axis compared to surface morphs [15]. At present, it is
55 unclear the relevance of this asymmetry, however, some studies suggest it may facilitate
56 lateral swimming preference, rheotaxis (orientation towards flow), foraging, shoaling,
57 predator avoidance, and mate-finding [7, 16-20].

58 *Sinocyclocheilus* are distributed across a vast 62,000 km² karstic area in Yunnan

59 and Guizhou Provinces and Guangxi Zhuang Autonomous Region [21, 22]. Based on
60 their habitat preference, these fish can be divided into three principal groups: troglobitic
61 (cave-restricted); troglophilic (cave-associated); and surface-dwelling [9]. It remains
62 unclear the extent to which the lateral line system has undergone changes associated
63 with these different habitats, however one study characterized neuromast size
64 differences between two *Sinocyclocheilus* species [20].

65 Here we examined numerical variation, lateral distribution and behavioural
66 differences associated with neuromasts in *Sinocyclocheilus*. Neuromasts may provide
67 functional compensation for eye loss, therefore we hypothesized that more severe
68 eye/vision loss may be associated with compensatory expansions of the lateral line
69 neuromasts. Specifically, troglomorphy was predicted to be associated with more, and
70 larger, neuromasts. Additionally, we anticipated a higher prevalence of distributional
71 asymmetry of neuromasts compared to surface fish, owing to relaxation of symmetry.

72 We found that neuromast distributions were asymmetric among all groups,
73 however the degree of asymmetry was most apparent for Regress-Eyed (collectively
74 both Blind and Micro-Eyed) species. Additionally, in phylogenetic contexts the pace of
75 neuromast evolution is faster among species with smaller eyes, compared to normal
76 eyed species. Taken together, this work provides the first diversification-wide
77 description of lateral line evolution, and clarifies the shared evolutionary pressure on
78 constructive trait evolution among distantly-related species that colonize caves.

79

80

81 **2. Methods**

82 *Sinocyclocheilus* adult fishes used in this study were examined using live, biosafe
83 staining techniques and behavioural assays. The project was approved by Guangxi
84 Autonomous Region Government and Guangxi University Ethical Clearance
85 Committee (# GXU-2021-125).

86 **(a) Fish maintenance in captivity**

87 Adult fish used in this study were collected from the field from 2017-2020 across
88 Yunnan and Guizhou Provinces and Guangxi Zhuang Autonomous Region of China
89 (figure 1, see geographic coordinates in electronic supplementary material: table S1,
90 figure S5). All fish were maintained in a centralized fish aquarium system, and
91 maintained at (pH: 7.0 - 8.0, temperature $19^{\circ}\text{C} \pm 1^{\circ}\text{C}$, dissolved oxygen 8.5mg/L).
92 Specimens larger than 5 cm were maintained in large glass aquaria ($90 \times 50 \times 50$ cm,
93 $150 \times 80 \times 80$ cm), with individual mechanical and bio-filters. For this study, 76
94 individuals from 26 *Sinocyclocheilus* species were used (table 1). *Carassius auratus* (n
95 = 3) and *Cyprinus carpio* (n = 3), two species from a closely related clade to
96 *Sinocyclocheilus* for comparison.

97

98

99

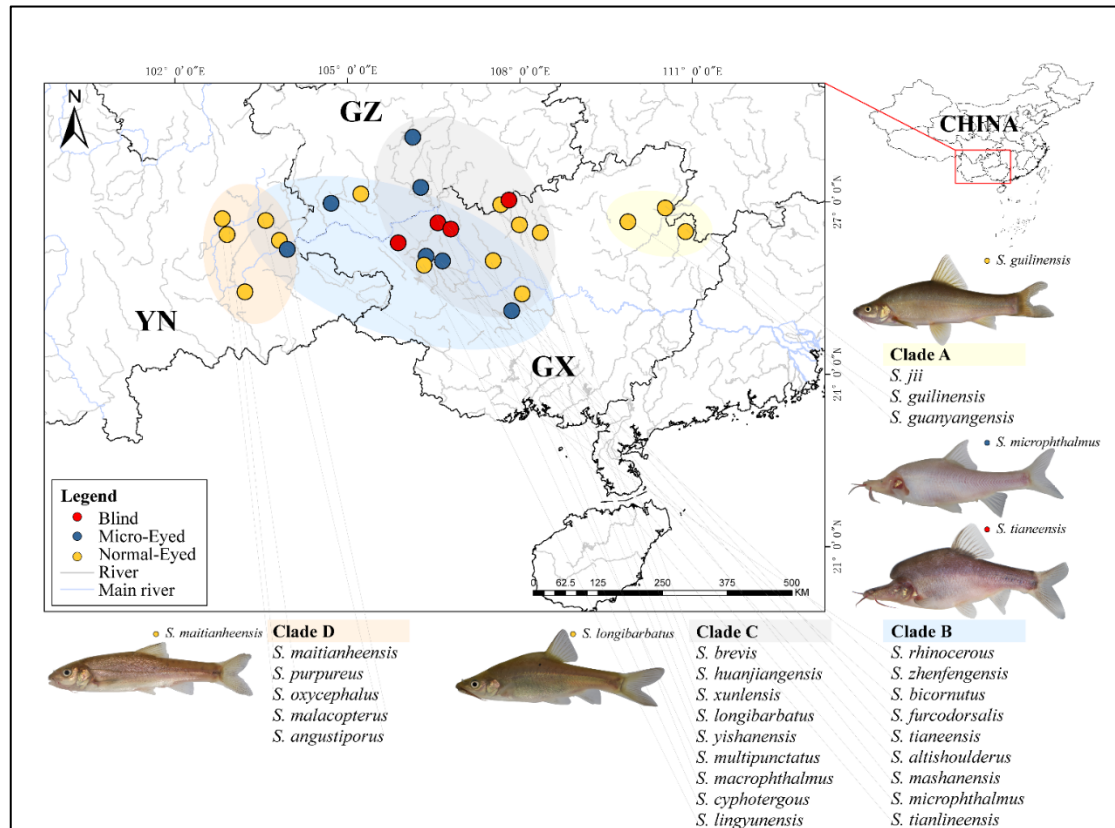
100

101

102

103 **Table 1.** Summary of 26 *Sinocyclocheilus* species used in the current analysis grouped
 104 according to eyes morphology and habitat.

	Troglobitic (TB)	Troglophilic (TP)	Surface (S)
Blind (B)	<i>S. furcodorsalis</i>		
	<i>S. tianlinensis</i>		
	<i>S. tianeensis</i>		
	<i>S. xunlensis</i>		
Micro-eyed (ME)	<i>S. mashanensis</i>		
	<i>S. altishoulderus</i>		
	<i>S. microphthalmus</i>	<i>S. multipunctatus</i>	
	<i>S. bicornutus</i>		
	<i>S. rhinoceros</i>		
	<i>S. cyphotergous</i>		
Normal-eyed (NE)	<i>S. guilinensis</i>		
	<i>S. huanjiangensis</i>		
	<i>S. macrophthalmus</i>		<i>S. angustiporus</i>
	<i>S. guanyangensis</i>		<i>S. oxycephalus</i>
	<i>S. brevis</i>	<i>S. longibarbatus</i>	<i>S. malacopterus</i>
	<i>S. lingyunensis</i>		<i>S. purpureus</i>
	<i>S. zhenfengensis</i>		<i>S. maitianheensis</i>
	<i>S. jii</i>		
	<i>S. yishanensis</i>		



105

106 **Figure 1. Map showing the distribution of sampling sites of the 26 species of**

107 ***Sinocyclocheilus* (n = 76) used in this study. These fishes are mainly distributed across**

108 **South China's Karstic habitats on three provinces: Guangxi Autonomous region (GX),**

109 **Guizhou (GZ) and Yunnan (YN). The four main clades (A – D, represented by a color**

110 **code), the species used from each clade, and a representative photo of species from**

111 **these clades are shown. Early emerging Clade A is mainly distributed in the eastern**

112 **range of the diversification and Clade D to the hills to the West; Clade B and C contain**

113 **the most troglomorphic species and are distributed mainly across GX and GZ. The eye-**

114 **condition (Blind, Micro-eyed and Normal-eyed) are depicted using a color code.**

115

116 **(b) Vital staining of neuromasts**

117 **To visualize bones and neuromasts, live fish were immersed in 1mg/L Calcein-AM**

118 (C0875-5G; Sigma-Aldrich) and 20 μ g/ml DASPEI (D0815; Sigma-Aldrich) [15, 23,
119 24]. Fish were anesthetized using MS222 (E808894-5g; Macklin) 0.01-0.02g/L for 3-6
120 min followed by brief immersion in ice water for ~20s, depending on size and age (e.g.,
121 smaller specimens were exposed to ice water for shorter periods). All individuals were
122 continuously monitored to ensure the health and safety of experimental individuals.

123 **(c) Digital Analysis of Neuromasts Position and between Distances**

124 This study focused on the cephalic region anterior to the opercular and interopercular
125 bones, near the arc on the lateral aspect [20, 22]. Images were collected using a Leica
126 M165FC fluorescent stereomicroscope outfitted with Leica Application Imaging
127 software (LAS X v3.4.2.18368). The dorsal, left and right aspects of each individual
128 were imaged under identical conditions. High-definition “montage” image were
129 consolidated following automated alignment and ‘flattening’ of 30 images collected in
130 the z-plane (\times 9/ 13/ 16 magnification) using LASX or Helicon Focus (Pro v7.6.1), to
131 perform the two-dimensional shape images. The use of montage imaging minimized
132 potentially confounding variables arising from the z-plane for each specimen.

133 The outline of fish and neuromast positions were obtained using the “Pencil” and
134 “Point” tool in GIMP (v2.10.24). Neuromast numbers were quantified using an
135 automated method in ImageJ (v1.8.0), following the method of Gross et al. (2016) [15].
136 For ambiguous images, we performed direct, manual counting (figure 3a). We
137 calculated the size (2-D area) of individual neuromasts, lens, and eye orbit diameter by
138 determining their size in pixels using the “measure” function in ImageJ and converting
139 to mm². We also used a vernier caliper to measure standard length (SL). To determine

140 the density of neuromast within particular unit areas, we used “Delaunay Voronoi”
141 triangulation in ImageJ to define a proxy for the mean distance between neuromasts
142 [25-27] (figure 3a).

143 **(d) Quantifying symmetry**

144 To examine positional symmetry of neuromasts across the left-right axis, we
145 manually superimposed the fluorescent images of neuromasts (figure 3b). We used
146 excitation filters for three colors (Blue 470/40 nm, Texas Red 560/40 nm and Green
147 546/10 nm). In GIMP, we then reflected the left images to align with the right images,
148 creating a single image. We measured the scoring of neuromasts in the reverse sequence
149 (right-side first) relative to the initial scoring of neuromasts (left-side first) to avoid bias
150 in our calculations [28].

151 The “colocalization” [29, 30], and “JACop” [31, 32] plugins in FIJI were used to
152 calculate an asymmetry coefficient [15, 33, 34]. We performed a Pearson’s correlation
153 to compare the intensity distribution between channels [35]. Next, we calculated an
154 Overlap Coefficient (OC), to identify positional overlap of signals from the left and
155 right sides [36]. This enabled us to quantify the extent to which positions of neuromasts
156 on the left and right sides of the cranium were symmetric (figure 3a).

157 We divided 26 species into Regressed-Eyed groups (containing Blind n = 12, and
158 Micro-Eyed n = 21) and Normal-Eyed groups (n = 45), following the categorization
159 and phylogeny of Mao et al. (2021). Importantly, a few *Sinocyclocheilus* species do not
160 have uniform eye sizes [22]. For instance, *S. guanyangensis* have highly variable eye
161 sizes, so for this study we selected individuals with the most normal eye morphology.

162 All parametric neuromast measures were subjected to one-way ANOVA with a post-
163 hoc Tukey test analysis. Non-parametric distributions were subjected to Wilcoxon
164 Signed Rank Test (2-tailed, Holm correction) or a Kruskal-Wallis test with a post-hoc
165 analysis Dunnett test (2-tailed, Bonferroni correction). Statistical significance was set
166 at $p < 0.05$. We used the packages “wmc” and “FSA” in R (v3.6.3). Principal
167 Component Analysis (PCA) was used to evaluate the following variables: number, area,
168 asymmetry coefficients and mean distance. To analyse the relationships between
169 Regressed-Eyed and Normal-Eyed groups, we performed Spearman’s rank correlation
170 coefficients using SL, eye traits, area, number, mean distance and OC of neuromasts
171 patterns.

172 **(e) Phylogenetic inference**

173 To study the patterns of neuromast evolution in *Sinocyclocheilus*, we inferred a
174 phylogenetic tree for the 26 species, using two available gene fragments from Genbank
175 (NADH-ubiquinone oxidoreductase chain 4 - ND4 and cytochrome b gene – Cyt b),
176 together with an outgroup species (*Cyprinus carpio*) (table S1). We used two different
177 methods for phylogenetic inference [37] – Bayesian and Maximum Likelihood for tree
178 construction (alignment, model selection and phylogenetic inference method details are
179 available in the electronic supplementary material, Supplementary Methods).

180 **(f) Evolution rate analysis**

181 To test the allometric evolution rate between neuromasts in different morphs [9],
182 we analysed neuromast numbers, left/right-side numbers, mean distance coefficient,
183 area and density (i.e. the proportion of number and area anterior to the gill). We used

184 100 potential trait histories from stochastic character mapping, and fit two alternative
185 models (single or multiple rate model, calculated by AIC) of evolution for each studied
186 trait. In the case of small samples, we assumed the AIC and AICc to assess, and then
187 weighted from Bayesian analyses on the trees using the brownie.lite function. We used
188 the package “rgl”, “ape” and “phytools” in R to calculate the model-averaged estimates
189 [38].

190 **(g) Patterns of neuromasts evolution using ancestral state reconstructions**

191 To understand the broad patterns of neuromast evolution in *Sinocyclocheilus*, we
192 classified 26 species into the following three morphological groups: (1) Left-right axis
193 asymmetry: according to different degree of overlapping coefficient, divided as
194 Absolute-asymmetry ($OC < 0.1$) and Slight-asymmetry ($OC \geq 0.1$) based on Gross et
195 al. (2016) [15]. (2) Left/right-bias handedness: we used the normalized SN number by
196 signed (directional) asymmetry rate: $SAR = \frac{R-L}{R+L} \times 100\%$ following Planidin et al. (2021)
197 [39], which suggests the presence of two morphological categories: Right-biased (SAR
198 > 0 , neuromasts on right-side mainly) and Left-biased (SAR < 0 , figure S1). (3)
199 Distance expansion: depending on the results of neuromasts mean distance coefficient,
200 we divided species into Scattered ($DEL > 0.2$) and Serried ($DEL \leq 0.2$), following
201 Gross et al. (2016) [15] (table S1).

202 To understand the evolution of neuromast patterns, we performed ancestral state
203 reconstructions using these three morphological categories. One hundred stochastic
204 reconstructions were simulated through the stochastic mapping approach that was
205 conducted using function “make.simmap” (model = “ER”) in the R packages “ape”,

206 “phytools” and “viridisLite”.

207 **(h) Cave-dwelling behaviour associated with neuromast variation**

208 To understand how neuromast patterns may facilitate certain behaviour, we carried out
209 a series of behavioural assays. All assays were performed using the following 14 species
210 (n = 3 individuals for each): Blind - *S. furcodorsalis*, *S. tianlinensis*, *S. tianeensis*;
211 Micro-Eyed - *S. mahanensis*, *S. microphthalmus*, *S. bicornutus*, *S. multipunctatus*;
212 Normal-Eyed - *S. guilinensis*, *S. longibarbatulus*, *S. macrophthalmus*, *S. oxycephalus*, *S.*
213 *zhenfengensis*, *S. purpureus*, *S. maitianheensis*. Each experimental fish was
214 acclimatized for 30 min in a rectangle assay arena (45 × 28 × 28 cm) in system water.
215 An infrared camera (Cannon XF400/405) was used to capture video under infrared light
216 in a quiet, dimly lit room (frame rate: 4Mbps (VBR, YCC 4:2:0, 25p, 1280 × 720).

217 Wall-following behaviour has been observed in *A. mexicanus* cavefishes; therefore,
218 we examined a range of wall-following within the arena. This included fish swimming
219 a minimum distance of its SL along the wall, or a distance of ≤ 0.5 SLs away from the
220 wall (figure 5a-b) [40, 41]. We recorded normal tracking without stimulation for 10-
221 min to determine if wall-following behaviour was present using EthoVision XT (v15.0 ,
222 Noldus) alongside direct visual monitoring. (2) We next used an aeration pump (45~50
223 Hz vibration) for 5-min to record the approaching of a novel object in modified
224 vibration attraction behaviour test [42-44]. We selected the area centered on the
225 stimulation model based on tank shape (10 × 16 cm). We monitored the frequency of
226 time spent in the stimulation range from left/right-side. Data analysis were performed
227 in R’s basic functions as mentioned.

228

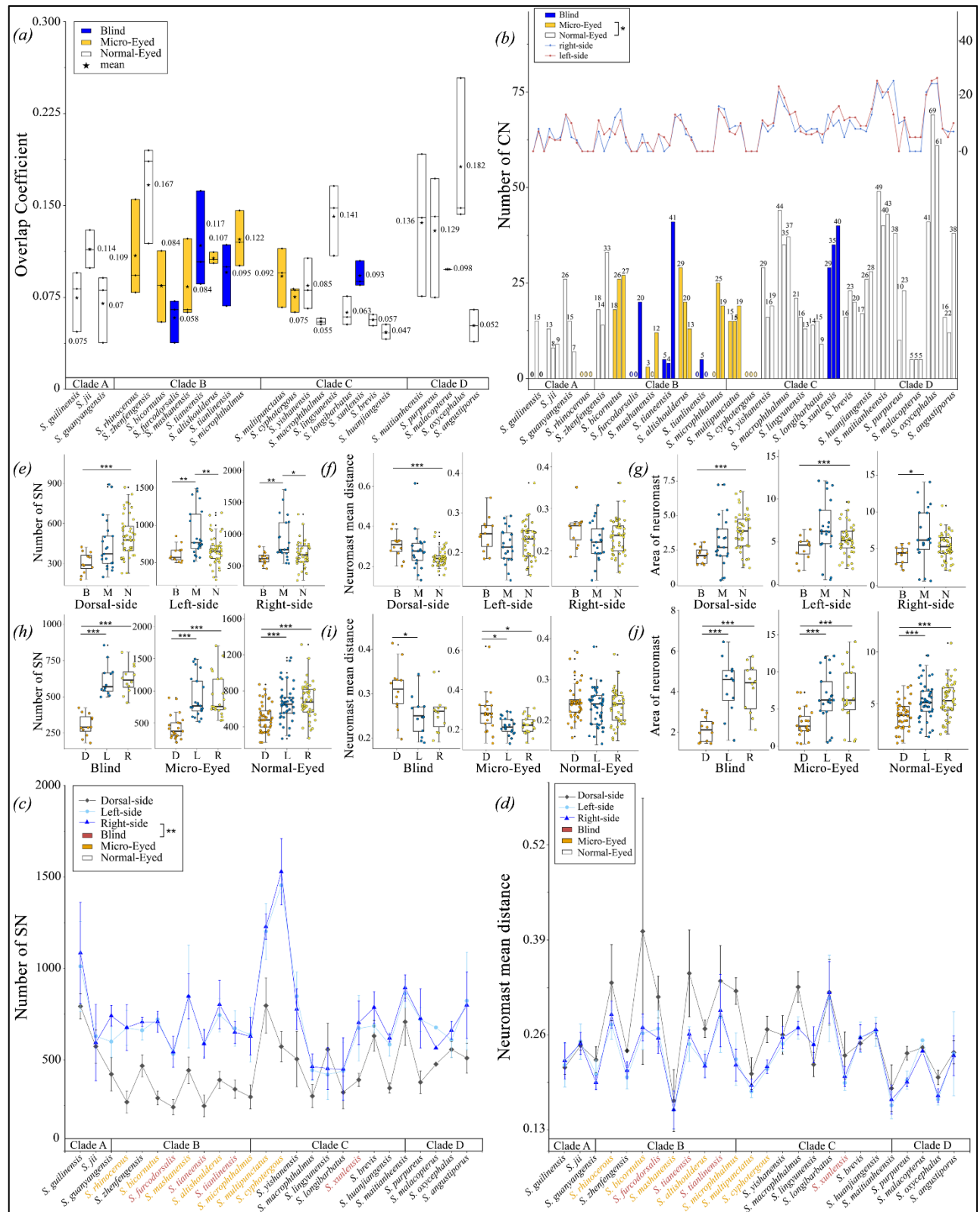
229 **Results and Discussion**

230 All cavefish species, for which neuromast distribution has been studied, are
231 asymmetric [15, 45-48]. Accordingly, we found the two outgroup species of Cyprinidae
232 did not show a comparable pattern of neuromast asymmetry as was observed in
233 *Sinocyclocheilus*. Fish living in perpetual darkness frequently lose vision while
234 enhancing non-visual sensation, such as the lateral line [42, 49, 50]. Here we show
235 that *Sinocyclocheilus* similarly conform to this pattern (figure 2). Additionally,
236 widespread neuromast distributional asymmetry in *Sinocyclocheilus* is convergent with
237 other distantly related cavefish species inhabiting similar cave microenvironments.
238 Interestingly, our results showed that this asymmetric neuromast pattern is variable
239 across the 26 *Sinocyclocheilus* species tested, with most species demonstrating a right-
240 sided bias (figure 4). Evidence for neuromast asymmetry patterns in other lineages
241 comes from two lineages from Central and North America: *Astyanax mexicanus*, with
242 a left-side bias and the *Gasterosteus aculeatus* (stickleback fish), with a right-side bias
243 [39, 51]. These results reveal variation in “sidedness” across taxa, despite convergence
244 in asymmetry.

245 **(a) Patterns of neuromast symmetry and asymmetry**

246 The neuromasts distribution pattern showed asymmetry across the left-right axis, with
247 variation both within and across species (figure 2a, table S2). Interestingly, mean
248 overlap coefficients indicated that all species showed a degree of neuromast asymmetry.
249 Normal-Eyed species showed the least asymmetry, while Blind species showed the

250 highest and Micro-eyed species had intermediate values (mean \pm s.d.: Normal-Eyed =
251 0.098 ± 0.05 ; Blind = 0.091 ± 0.031 ; Micro-eyed = 0.096 ± 0.027 ; $H_2 = 0.64$, $p > 0.05$).
252 This finding is consistent with prior work suggesting that asymmetry may facilitate
253 navigation in darkness [52, 53], foraging [54] and the ability to maximize sensory
254 information using fewer receptors [39, 51]. In comparing asymmetry measures across
255 clades, Clade D (all Normal-Eyed living in surface, showed as: N-S; mean \pm s.d. =
256 0.119 ± 0.058) showed the least asymmetry, while Clade C (mean \pm s.d. = 0.079 ± 0.031)
257 showed the highest asymmetry; with Clade A and B demonstrating intermediate values
258 (Clade A – 0.086 ± 0.029 and Clade B – 0.104 ± 0.038).
259



260

261 **Figure 2. Comparison of neuromast-related measurements for 26 species of**

262 ***Sinocyclocheilus* (n = 76).**

263 (a) The average scores of Overlapping Coefficient (OC) measured as the pattern of

15

264 neuromasts on left/right-side of the fish. The standard of asymmetry results is defined
265 as: asymmetry ($OC < 0.1$), symmetry ($OC \geq 0.1$). Clade A-D represent the clade level
266 relationships of these 26 species in the phylogenetic tree. All statistical results are
267 available in table S1, S2.

268 (b) The bars represent the individual's canal neuromasts (CN) total counts and the lines
269 represent the left and right sides of cephalic CN in different species. The CN of Micro-
270 Eyed species was significantly less than Normal-Eyed species ($H = -2.64$, $p = 0.025$).

271 (c) The mean number of superficial neuromasts (SN) on the cephalic area (dorsal, left
272 and right sides) in different *Sinocyclocheilus* species.

273 (d) The mean surface area covered by SN on the dorsal/left/right-side of different
274 *Sinocyclocheilus* species. The surface species covered by the dorsal SN are less than
275 that of the surface are covered by the right and left sides of fish.

276 (e-g). The comparisons about: (e) the number of SN; (f) neuromasts mean distance
277 coefficient; (g) area of SN on Dorsal/Left/Right-side on cephalic area. Group divided
278 by the Blind (B in orange), Micro-Eyed (M in blue) and Normal-Eyed (N in yellow).

279 The Wilcoxon signed rank (2-tailed, Holm correction) test suggested that the surface
280 covered by dorsal neuromasts are significantly less than that covered by the right and
281 left sides. *: $P < 0.05$, **: $P < 0.01$, and ***: $P < 0.001$. All statistical results are
282 available in table S2, S5.

283 (h-j). The comparisons of the non-parametric statistical tests performed for (h), the
284 mean number of SN; (i) neuromasts mean distance coefficient; (j) mean area of SN on
285 the cephalic area of the Blind, Micro-Eyed and Normal-Eyed morphs. The comparisons

286 were sub-divided into dorsal-side (D in orange), left-side (L in blue) and right-side (R
287 in yellow) for visualization purposes.

288

289 **(b) Patterns of neuromast distribution**

290 Generally, we found more SNs on the right compared to the left-side, however we
291 observed substantial variation between and across species. We examined distributions
292 in three aspects: dorsal, left and right sides. In the dorsal aspect, Blind fish have the
293 least, Normal-Eyed fish have the most, and the Micro-Eyed group was intermediate
294 (figure 2e). Unexpectedly, there were significantly fewer SNs in Blind species (mean \pm
295 s.d.: Blind = 1543 ± 248 ; Micro-Eyed = 2252 ± 802 ; Normal-Eyed = 1859 ± 504 ; $H_2 =$
296 10, $p = 0.0065$, table S5). In terms of lateral distribution, Blind and Normal eyed fish
297 had higher numbers on the right-side, while Micro-Eyed species had more neuromasts
298 on the left-side (median: left = 767, right = 758; $W = 227$, $p = 0.890$; figure 2h; table
299 S5).

300 We found that dorsal neuromast numbers are significantly lower than the lateral
301 sides. An interesting exception was *S. linyunensis* (N-TB, Clade C), dorsally
302 distributed neuromasts outnumbered laterally-situated neuromasts (mean dorsal = 557,
303 left = 419, right = 453; figure 2c, table S5). In the dorsal aspect, Normal-Eyed species
304 had the most neuromasts, while the Blind group had the fewest. One potential
305 explanation for this difference could be that obligate subterranean fishes experience
306 relaxed selective pressure (e.g. aerial predation from birds) [21, 55], but perhaps dorsal
307 neuromasts are necessary for navigation within caves [56].

308 With respect to neuromast expansion (scatter), we found that the most scattered
309 SNs are dorsal, especially in Blind species (mean \pm s.d.: Blind = 0.31 ± 0.06 ; Micro-
310 Eyed = 0.28 ± 0.10 ; Normal-Eyed = 0.24 ± 0.04 ; $H_2 = 12$, $p = 0.002$; figure 2f, table
311 S5). Additionally, neuromasts tend to be more scattered on right- compared to the left-
312 side across all three groups (median right/left Blind = 0.26, 0.25; Micro-Eyed = 0.22,
313 0.21; Normal-Eyed = 0.24, 0.23; figure 2d). Interestingly, the Blind cavefish group
314 demonstrated the most scatter, while the Micro-Eyed group had the least scatter (figure
315 2i, table S5). In Mexican cavefish, *Astyanax* demonstrates more scatter in the surface
316 forms compared to *Sinocyclocheilus* [15, 57], however this is likely due to the fact that
317 *Astyanax* Blind forms have more neuromasts, and hence less scatter.

318 In the comparison of surface area covered by neuromasts, we found a significantly
319 lower surface area populated by neuromast dorsally, with the Blind group having the
320 smallest area (mean \pm s.d. Blind = 2.14 ± 0.59 ; Micro-Eyed = 3.13 ± 1.94 ; Normal-
321 Eyed = 3.88 ± 1.33 ; $H_2 = 15.9$, $p = 0.0003$; figure 2j). When comparing lateral sides,
322 we found the total distributional area of neuromasts to be highly comparable within
323 groups (median right/left-side Blind = 4.44, 4.6; Micro-Eyed = 6.19, 6.21; Normal-
324 Eyed = 5.31, 5.14; table S5). Normal-Eyed species have the largest area of neuromast
325 distribution, Micro-Eyed fish have an intermediate area, and the Blind group had the
326 smallest area covered by (mean \pm s.d. = 10.56 ± 2.95 ; Micro-Eyed = 16.44 ± 8.80 ;
327 Normal-Eyed = 14.49 ± 4.59 ; $F = 3.83$, $p=0.026$; figure 2g). Although it has been shown
328 that the neuromast complexity of the Blind species is greater than Normal-Eyed species,
329 this however, has not been established at a diversification-wide scale.

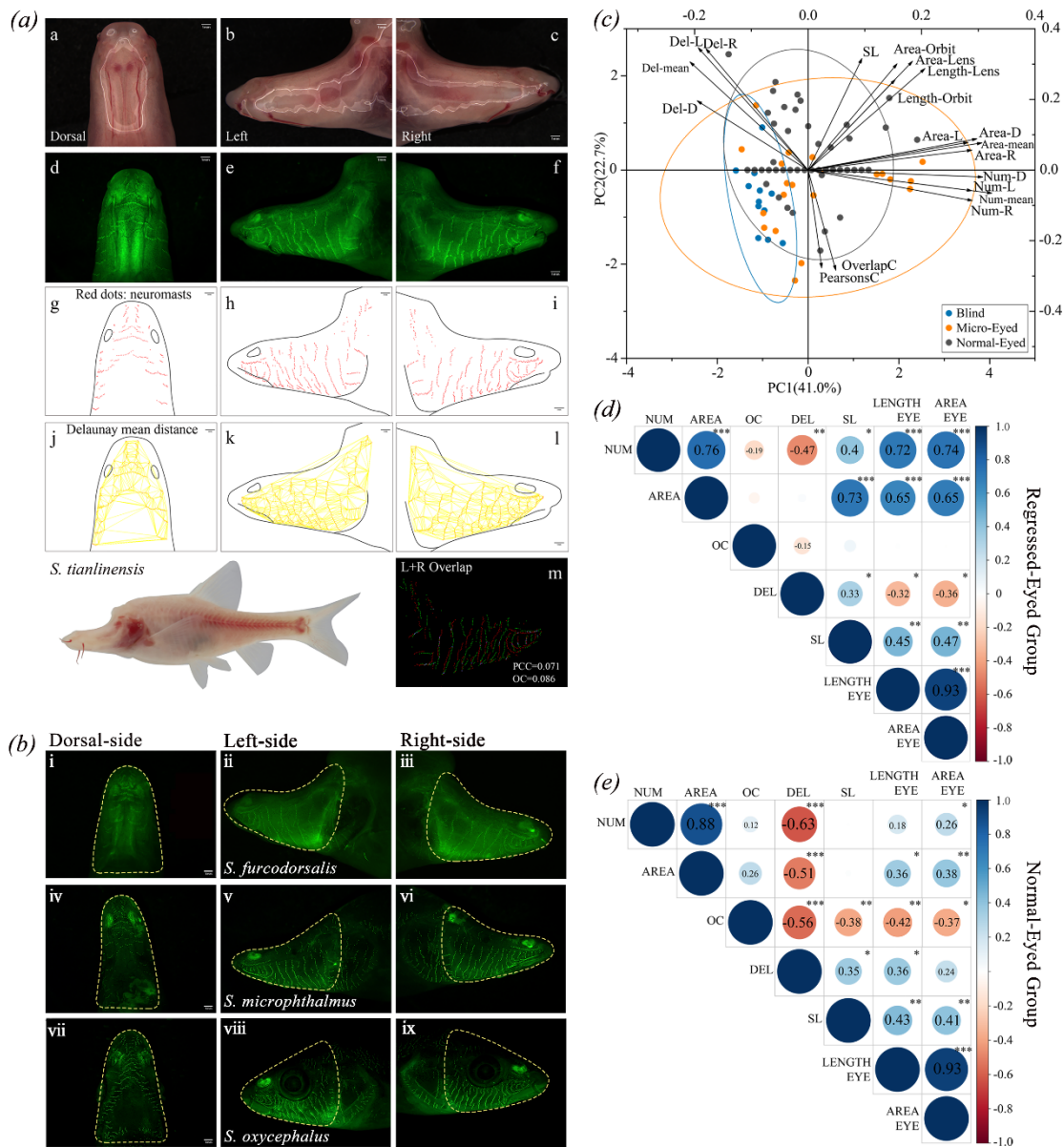
330 Blind *Sinocyclocheilus* have fewer CNs compared to Normal-Eyed
331 *Sinocyclocheilus* (median Blind = 5, Micro-Eyed = 13; Normal-Eyed = 17; table S5),
332 reflecting the same pattern as SNs. For *Astyanax*, surface fish are invariant in terms of
333 numbers, but cavefish are highly variable. Surprisingly, two species, *S. rhinoceros*
334 and *S. cyphotergou* appeared to possess no CNs (both M-TB, figure 2b), suggesting
335 the canal lateral line system may have regressed in this species. Interestingly, a similar
336 phenomenon has been observed in Amblyopsid cavefish (Teleostei: Percopsiformes)
337 [47] and in Threespine Sticklebacks (*Gasterosteus aculeatus*) [58].

338 In sum, neuromasts are generally reduced in number and area in Blind species, but
339 not in scatter (expansion). Somewhat surprisingly, Micro-Eyed species had the most
340 neuromasts, greater area, and least dense distribution of neuromasts. We propose that
341 Blind species may have optimized adaptation to the subterranean biome by using fewer,
342 but more complex, neuromasts. Blind *S. tianlinensis*, for instance, have SNs with
343 greater diameters and more hair cells compared to Normal-eyed *S. macrophthalmus*
344 [20].

345 (c) Correlations between asymmetry and eye condition

346 We performed a Spearman Rank's correlation of the highly loading variables for
347 the Regressed-Eyed and Normal-Eyed. In the Regressed-Eyed group, eye measures
348 demonstrated a significantly positive correlation with neuromasts number ($\rho= 0.7$, $p <$
349 0.001) and area ($\rho= 0.7$, $p < 0.001$), but a slightly negative correlation with mean
350 distance between neuromasts ($\rho= -0.3$, $p < 0.05$). In the Normal-Eyed group, eye
351 measures had a significantly positive correlation with neuromasts area ($\rho= 0.4$, $p <$

352 0.005) and mean distance ($\rho=0.4$, $p < 0.05$), but significantly negative correlation with
 353 the results of asymmetry ($\rho= -0.4$, $p < 0.001$; figure 3d,e, table S4). Overall, the
 354 Regressed-Eyed group is more asymmetric compared to Normal-Eyed group.



355

356 **Figure 3. Summary of fluorescent staining results for different cavefish morphs.**

357 (a) the fluorescent staining results of *S. tianlinensis* (Blind species-Troglobitic, B-TB).

358 (table 1 & table S1).

359 (a-c) photos taken under normal lights. (d-f) dorsal, left and right sides of the

360 neuromasts under fluorescent light. (small green dots are SN, bigger green dots are CN).

361 (g-i) The diagrammatic representations of the dorsal, right and left side neuromasts.

362 SNs denoted by red dots and the area outlined in black represent cephalic region and

363 the olfactory area. (j-l) The neuromasts mean distance measures as the “Delaunay Mean

364 Distance” are indicated by yellow lines. (m) The asymmetry values calculated by

365 overlap coefficient. Red and green dots represent the left and right sides of the fish.

366 Note that the scale of the images is the same at the length of 1.0 mm.

367 (b) The results of the fluorescent staining of three cavefishes, (i-iii) *S. furcodorsalis*,

368 (iv-vi) *S. microphthalmus* and (vii-ix) *S. oxycephalus*, used as representatives of each

369 eye-related morphs. These three species are classified as (B-TB), Absolute-

370 asymmetry/Scattered/Left-bias; (M-TB), Slight-asymmetry/ Scattered/Right-bias and

371 (N-S), Slight-asymmetry/Serried/Right-bias respectively. Scales of the images are the

372 same at the length of 1.0 mm.

373 (c) Principal Component Analysis (PCA) bi-plot for the distribution traits of neuromasts

374 in *Sinocyclocheilus*.

375 The dorsal/left/right-side and mean counts number (Num-D, Num-L, Num-R, NUM);

376 dorsal/left/right-side and mean distance coefficient (Del-D, Del-L, Del-R, DEL);

377 asymmetry coefficients of neuromasts (PearsonsC, OverlapC); eyes traits (area of

378 lens/orbit (Area-Lens, Area-Orbit) and length of lens/orbit (Length-Lens, Length-

379 Orbit)) with standard length [5] were included as variables in the PCA. All results are

380 available in Supplemental table S2, S3.

381 (d) The Correlations between SN number (NUM), area (AREA), mean distances

382 coefficient (DEL) and asymmetry coefficient (OC) of neuromasts; standard length [5]
383 and the length of lens (LENGTHEYE) and area of lens (AREAEYE). The scores
384 indicate the results of the spearman's rank correlation coefficient $|\rho|$; $< 0.3 =$ no
385 correlation, $0.3-0.8 =$ low correlation, $> 0.8 =$ high correlation. Positive correlations ($\rho >$
386 0) and negative correlations ($\rho \leq 0$) are shown in blue and red colors respectively. *: P
387 < 0.05 , **: $P < 0.01$, and ***: $P < 0.001$ indicate the level of statistical significance. All
388 results are available in table S4.

389

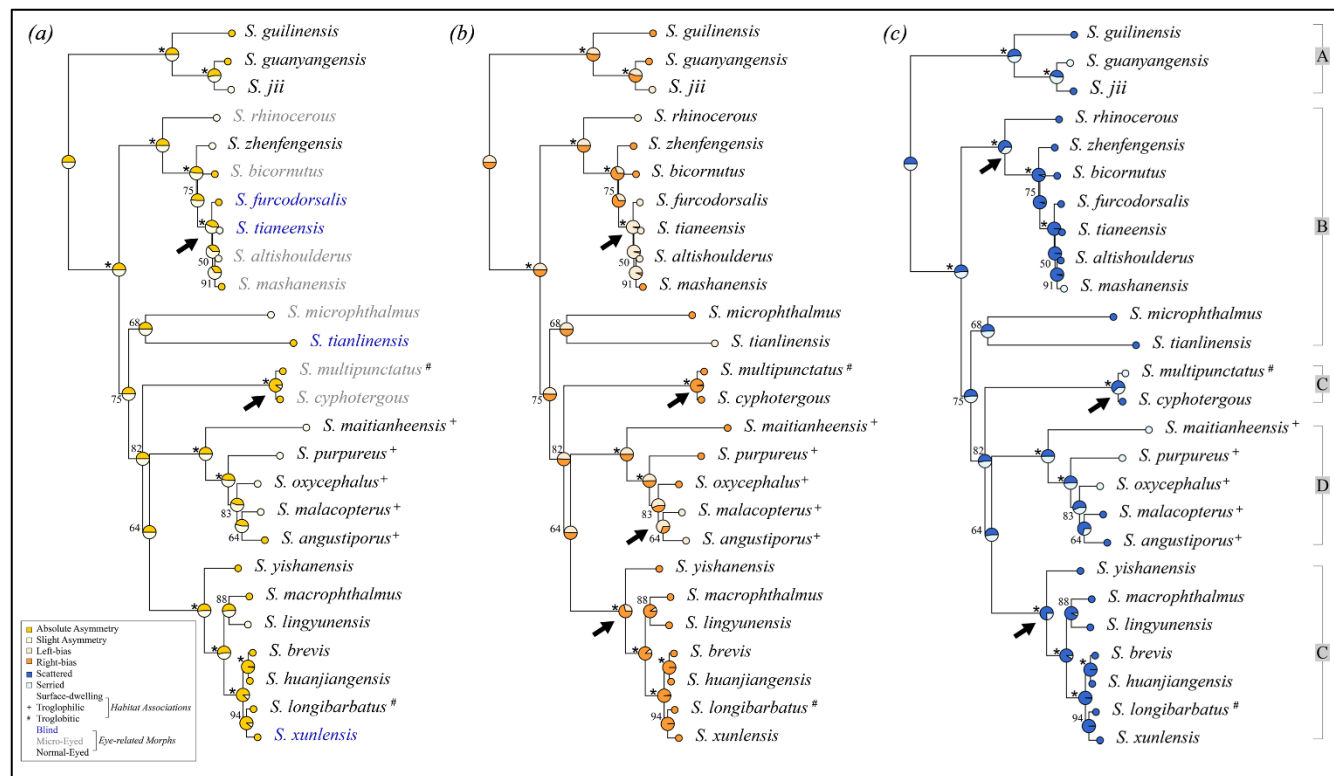
390 **(d) Dimensionality of the neuromast variables**

391 We performed a principal component analysis (PCA) based on 26 species of
392 *Sinocyclocheilus* and their neuromast-related variables, to identify key features
393 underlying neuromast variation. PC1 was explained mostly by the number of
394 neuromasts (mean number: NUM, counts on dorsal side: Num-D) and the total
395 neuromast distributional area (AREA). PC2 was explained mostly by the distances
396 between neuromasts (mean distance coefficient on left side: Del-L, on right side: Del-
397 R; table S3). The 95% confidence intervals for each group shows that intraspecific
398 variation in Blind group were the narrowest, while the Micro-Eyed group showed the
399 highest variation (figure 3c). This may be explained by the fact that Micro-Eyed forms
400 are subjected to selective pressures of both surface habitats, subterranean habitats and
401 the transitional habitats between these [22, 59, 60]; i.e. habitat heterogeneity.

402

403 **(e) Patterns of neuromasts evolution**

404 We next performed an ancestral reconstruction for three character states: asymmetry,
 405 handedness and neuromasts expansion. We found the deeper nodes in the phylogeny
 406 showed ambiguity for asymmetry and handedness (see maximum credibility tree;
 407 figure 4). However, the deeper nodes for neuromast distribution suggested a scattered
 408 distribution of neuromasts is the ancestral condition. In *Sinocyclocheilus*, ~ 70% of
 409 the species examined demonstrate right-handedness. Our ancestral state
 410 reconstruction shows an entire clade of 7 species is right-handed. However, both left-
 411 and right-handed mixed clades and sister taxa are present within the diversification,
 412 suggesting this is a variable trait. In contrast, ancestral state reconstructions show
 413 nearly 80% of the *Sinocyclocheilus* have scattered neuromast distributions.
 414 Additionally, all Blind species showed a scattered neuromast pattern of distribution.
 415 (figure 4c; black arrow).



416

417 **Figure 4. Patterns of cephalic neuromast trait evolution of *Sinocyclocheilus* based**

418 **on ancestral state reconstruction on the maximum-likelihood tree.** Ancestral state

419 reconstructions based on the Bayesian inference method is shown in figure S2-S4.

420 (a) Ancestral state reconstruction using stochastic character mapping for symmetry in

421 neuromasts pattern (Absolute/Slight-asymmetry). The tip colors represent state of the

422 extant species and each node indicates the ancestral state as a proportion of the tip state.

423 A, B, C and D showed on the extreme right of the figure indicate four major clades.

424 The bootstrap values > 95% are indicated as * on nodes.

425 (b) Ancestral state reconstruction using stochastic character mapping for handedness

426 bias (Left/Right-bias) on the phylogeny.

427 (c) Ancestral state reconstruction using stochastic character mapping for neuromast

428 expansion (Scattered/Serried) on the phylogeny.

429

430 **(f) Evolution rates analysis**

431 Among cavefish, the rate of neuromast evolution has only been determined for

432 *Sinocyclocheilus*. The rate of scatter for Blind species is higher compared to others

433 (mean distance and density - 3.5 and 6.8 times increased than Normal-Eyed species),

434 and the rate of numerical expansion of neuromasts is 1.2 times greater in Micro-Eyed

435 species (table 3). Normal-Eyed *Sinocyclocheilus* species demonstrated lower

436 evolutionary rates for every character state. A multiple-rate model of evolution

437 provided the best fit for mean distance between neuromasts, relative neuromast

438 density and neuromast distribution area. However, a single-rate model of evolution

439 provided the best fit for traits associated with neuromast numbers (table S6). Thus, the

440 evolutionary rate of cave-related neuromast patterns were highest in cave adapted
441 forms. Further, rates of evolution for surface area covered by SN neuromasts, and
442 right-sided neuromast numbers, are moderately increased in Blind and Micro-Eyed
443 species.

444 **Table 2.** Model-averaged rate parameters for the measured traits of neuromasts in
445 eyes-related morphs of *Sinocyclocheilus* species. **Bold font** = highest rate

446

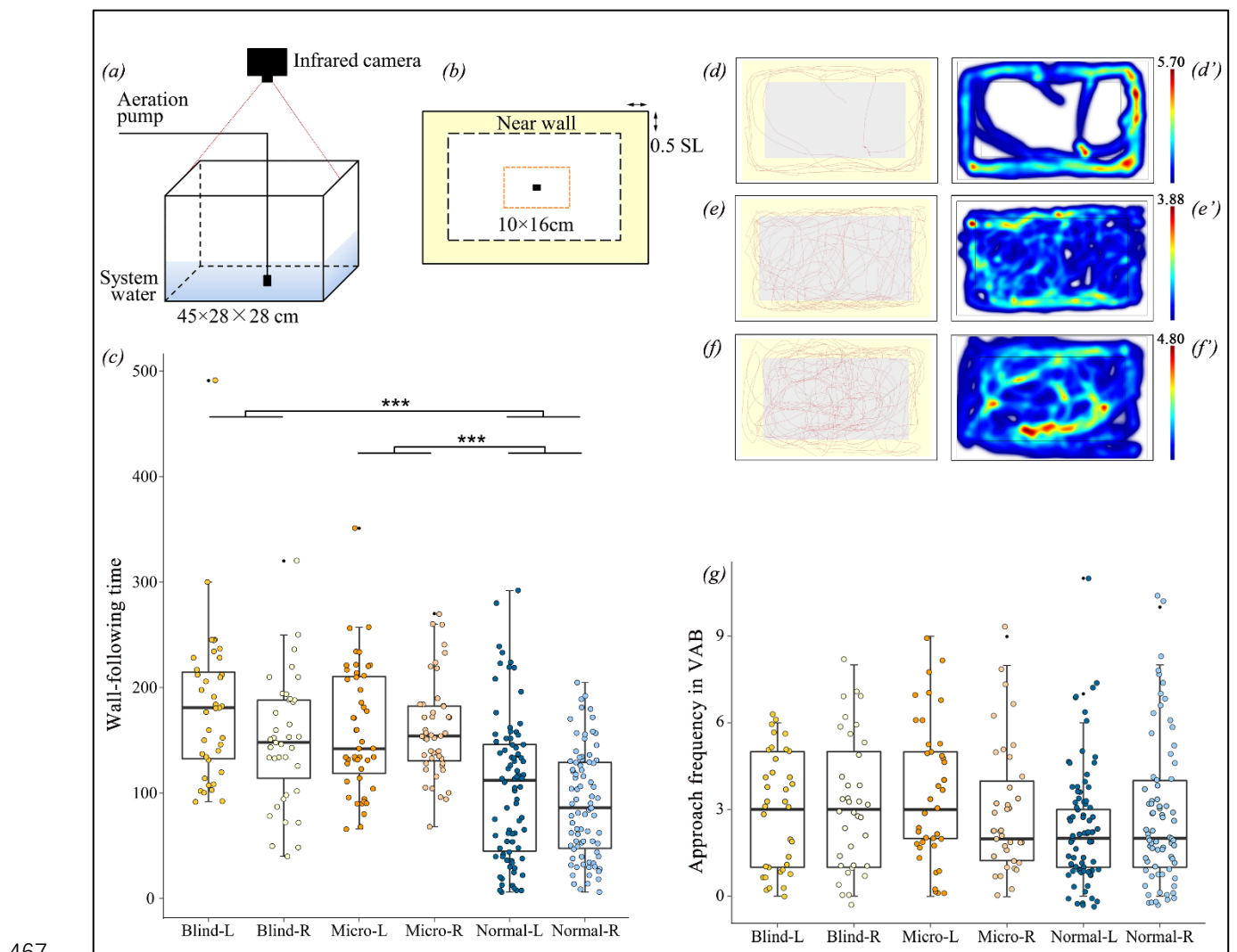
Trait	Average rate		
	Blind	Micro-Eyed	Normal-Eyed
Number	155.1042	179.4815	150.6202
Left Number	0.6395	0.4106	0.4249
Right Number	0.7095	0.5056	0.5329
Area	102.8836	106.2819	101.9520
Mean distance	34.4129	11.7357	7.9001
Density	362.2959	64.3977	42.2944

447 **(g) Behavioural correlates of neuromasts**

448 We performed a series of behavioural assays, and found that Blind species
449 navigate markedly differently from eyed-species. Blind species have a well-
450 established wall-following behaviour, while sighted species utilize an entire arena
451 space (figure 5). We found that Blind species prefer to use the side with fewer
452 neuromasts for wall-following, but the side with more neuromasts for exploring (i.e.,
453 stimulation during VAB test). Micro-Eyed species having a left-bias in neuromast
454 distribution, and approached a stimulation area from the left-side (median = 4) more
455 frequently than right-side (median = 3; $W = 612$, $p > 0.05$). These species, however,
456 followed the wall on their right-side (median = 154) for a significantly longer time
457 compared to the left-side (median = 142; $W = 967$, $p < 0.001$; figure 5c,g; table S5).

458 Behavioural heatmaps depicting wall-following behaviour showed that Blind species
459 prefer swimming in a fixed route, but eyed-species swam in irregular patterns (figure
460 5 d-f').

461 Wall following behaviour has also been characterized in *Astyanax mexicanus*. In
462 this species, blind morphs similarly use the side with fewer neuromasts towards the
463 wall, perhaps to use the contralateral side for detecting stimuli important for feeding,
464 communication and spatial learning [17, 42]. This divergence occurred during the
465 geological uplift of the Yunnan-Kweichow Plateau together with the aridification of
466 China, which occurred during the Pliocene and the Pleistocene [61]



468 **Figure 5. The experimental setup and results of the behavioural assays.**

469 (a) Schematic diagram showing the assay system used to for the wall-following and
470 vibration attraction behaviour (VAB).

471 (b) The vertical view of the arena's schematic diagram. The pale yellow area within the
472 dotted line depict the near-wall belt ("Near wall"). The orange dotted line showed the
473 stimulating area. The black rectangle in center shows the Aeration pump.

474 (c) The boxplot showing a comparison of the wall following time of Blind (3 species;
475 n = 9), Micro-Eyed (4 species; n = 12) and Normal-Eyed (7 species; n = 21) morphs.
476 Their handedness was also considered and the Kruskal-wallis Rank Sum Tests showed
477 that the groups spent significantly different ($U = 79.49$, $p < 0.001$) times following the
478 wall. Levels of significance indicated by ***.

479 (d-f'). Representative result of a 10-min wall-following behaviour assay for three
480 species. Vertical view of the swimming path of Blind fish (d,d'; *S. tianeensis*, B-TB),
481 Micro-Eyed fish (e,e'; *S. microphthalmus*, M-TB) and Normal-Eyed fish (f,f'; *S.*
482 *macrophthalmus*, N-TB).

483 (d, e, f) Visualization of the traces of the fish swimming paths as depicted by EthoVision.
484 (d', e', f') Heatmaps generated from the trial results of the wall-following behaviour.
485 The color bar represents the total time (min) the fish stayed in one place. Warmer colors
486 denote areas with a longer time spent, whereas cooler colors denote areas of shorter
487 time spent.

488 (g) The results of the frequency of approach in stimulation area of VAB test.

489

490 *Sinocyclocheilus* is an ancient species complex, with an estimated age for the
491 clade of nearly 10-11 Mya [9, 62]. They are distributed across an enormous karstic
492 area spanning three provinces [21]. One of the main forms of speciation seems to be
493 isolation of populations over long periods, and therefore geographic speciation
494 appears to have dominated this diversification [61]. The neuromast variability seen in
495 these fishes is most likely attributable to the collective influences of both selection-
496 and drift-related evolutionary mechanisms that have played on these fishes over long
497 periods. However, the exact dynamics of the evolution of neuromasts is still an
498 intriguing question to be explored.

499

500 **Conclusion**

501 In *Sinocyclocheilus*, alongside some basic patterns, there is widespread variation in
502 cephalic neuromast patterns between species and to some extent within species. We
503 showed neuromast asymmetry with right-side enhanced for most species. For almost
504 all species, the dorsal neuromast numbers were lesser than either of the sides.
505 Furthermore, Regressed-Eyed (Blind and Micro-Eyed) species are more asymmetric
506 than the Normal-Eyed forms. Interestingly, we found the greatest degree of neuromast
507 variation and rate of evolution in Micro-Eyed species (living outside and inside caves
508 - troglomorphic), this is possibly an adaptation for life in two markedly different habitats
509 types. Assays of swimming behaviour suggest a functional role of neuromasts in
510 habitat exploration. These patterns of neuromast distribution and swimming
511 behaviours are convergent with other cavefish lineages. The diversity of patterns and

512 variation can be explained by the deep evolutionary history associated with the karstic
513 region and the associated traits of this remarkable diversifications of fishes.

514

515 **Abbreviations Section:**

516 TB: Troglitic; TP: Troglitic; S: Surface; B: Blind; M: Micro-Eyed; N: Normal-
517 Eyed; CN: Canal neuromast; SN: Superficial neuromast; GXU: Guangxi University;
518 SL: Standard length; DEL: Delaunay Mean Distance (neuromast mean distance
519 coefficient); L: Left-Side; R: Right-Side; D: Dorsal-Side; PCC: asymmetry coefficient
520 1 = Pearson's Correlation Coefficient; OC: asymmetry coefficient 2 = Overlap-
521 Coefficient; PCA: Principal component analysis; AIC: Akaike information criterion;
522 mtDNA: Mitochondrial DNA; ND4: NADH-ubiquinone oxidoreductase chain 4; Cyt
523 b: cytochrome b gene.

524

525 **Declarations**

526 **Acknowledgements:** We thank the following individuals: members of EDD lab for
527 their cooperation and support; Chenghai Fu for assistance in the field; Gajaba Ellepola
528 for suggestions with the data analyses.

529

530 **Funding**

531 This work was supported by the (1) Startup funding for MM through Guangxi
532 University for fieldwork, lab work and student support. (2) National Natural Science
533 Foundation of China (#31860600) to JY for lab and fieldwork. (3) BC, TM and YL

534 were supported also by Innovation Project of Guangxi Graduate Education
535 YCBZ2021008. These funding bodies played no role in the design of the study and
536 collection, analysis, and interpretation of data or in the writing of the manuscript.

537

538 **Conflicts of interest/Competing interests**

539 We declare no conflicts of interest.

540

541 **Ethics approval**

542 The project was approved by Guangxi Autonomous Region Government and Guangxi
543 University Ethical Clearance Committee (protocol number: GXU-2021-125).

544

545 **Consent to participate**

546 Not applicable.

547

548 **Availability of data and material**

549 All the data used in the study are provided in the electronic supplementary material.

550

551 **Authors' contributions**

552 Conceptualization – MM, BC, JBG; Fieldwork – YL, BC, TM, MM, JY;

553 Experimentation and Lab Work – BC, XL; Data Analyses – BC, TM, WD, XL;

554 Interpretation – All; Figures – BC, WD, TM; Writing original draft – BC, MM, JBG;

555 Subsequent Drafts – All; Funding acquisition – MM, JY, BC, TM, YL; Supervision –

556 MM, JBG, JY.

557

558 **References**

- 559 1 Jeffery WR. 2001 Cavefish as a model system in evolutionary developmental biology. *Dev. Biol.* **231**,
560 1-12. (doi:10.1006/dbio.2000.0121)
- 561 2 Berti R, Durand JP, Becchi S, Brizzi R, Keller N, Ruffat G. 2001 Eye degeneration in the blind cave-
562 dwelling fish *Phreatichthys andruzzii*. *Can. J. Zool.* **79**, 1278-1285. (doi:10.1139/z01-084)
- 563 3 Jeffery WR. 2009 Regressive evolution in *Astyanax* cavefish. *Annu. Rev. Genet.* **43**, 25-47.
564 (doi:10.1146/annurev-genet-102108-134216)
- 565 4 Niemiller ML, Fitzpatrick BM, Miller BT. 2008 Recent divergence with gene flow in Tennessee cave
566 salamanders (Plethodontidae: *Gyrinophilus*) inferred from gene genealogies. *Mol. Ecol.* **17**, 2258-2275.
567 (doi:10.1111/j.1365-294X.2008.03750.x)
- 568 5 Jeffery WR, Strickler AG, Guiney S, Heyser DG, Tomarev SI. 2000 *Prox 1* in eye degeneration and
569 sensory organ compensation during development and evolution of the cavefish *Astyanax*. *Dev. Genes
570 Evol.* **210**, 223-230. (doi:10.1007/s004270050308)
- 571 6 Wilkens H, Strecker U. 2003 Convergent evolution of the cavefish *Astyanax* (Characidae, Teleostei):
572 genetic evidence from reduced eye-size and pigmentation. *Biol. J. Linn. Soc.* **80**, 545-554.
573 (doi:10.1111/j.1095-8312.2003.00230.x)
- 574 7 Yoshizawa M, Jeffery WR. 2011 Evolutionary tuning of an adaptive behavior requires enhancement
575 of the neuromast sensory system. *Commun. Integr. Biol.* **4**, 89-91. (doi:10.4161/cib.14118)
- 576 8 Yang JX et al.. 2016 The *Sinocyclocheilus* cavefish genome provides insights into cave adaptation.
577 *BMC Biol.* **14**, 1. (doi:10.1186/s12915-015-0223-4)
- 578 9 Mao TR, Liu YW, Meegaskumbura M, Yang J, Ellepola G, Senevirathne G, Fu C, Gross JB, Pie MR.
579 2021 Evolution in *Sinocyclocheilus* cavefish is marked by rate shifts, reversals, and origin of novel traits.
580 *BMC Ecol. Evol.* **21**, 45. (doi:10.1186/s12862-021-01776-y)
- 581 10 Cahn PH. 1989 The mechanosensory lateral line: neurobiology and evolution. *BioScience.* **40**, 215-
582 216. (doi:10.2307/1311373)
- 583 11 Webb JF, Shirey JE. 2003 Postembryonic development of the cranial lateral line canals and
584 neuromasts in zebrafish. *Dev. Dynam.* **228**, 370-385. (doi:10.1002/dvdy.10385)
- 585 12 Fritsch B, Wahnschaffe U. 1983 The electroreceptive ampullary organs of urodeles. *Cell Tissue Res.*
586 **229**, 483-503. (doi:10.1007/BF00207693)
- 587 13 Smith S. 1996 Pattern formation in the urodele mechanoreceptive lateral line: What features can be
588 exploited for the study of development and evolution? *Int. J. Dev. Biol.* **40**, 727-733. (doi:10.1016/0141-
589 8130(96)01109-9)
- 590 14 Bird NC, Webb JF. 2014 Heterochrony, modularity, and the functional evolution of the
591 mechanosensory lateral line canal system of fishes. *EvoDevo.* **5**, 21. (doi:10.1186/2041-9139-5-21)
- 592 15 Gross JB, Gangidine A, Powers AK. 2016 Asymmetric facial bone fragmentation mirrors asymmetric
593 distribution of cranial neuromasts in blind Mexican cavefish. *Symmetry.* **8**, 118.
594 (doi:10.3390/sym8110118)
- 595 16 Elipot Y, Hinaux H, Callebert J, Rétaux S. 2013 Evolutionary shift from fighting to foraging in blind
596 cavefish through changes in the serotonin network. *Curr. Biol.* **23**, 1-10. (doi:10.1016/j.cub.2012.10.044)
- 597 17 Yoshizawa M. 2015 Behaviors of cavefish offer insight into developmental evolution. *Mol. Reprod.*

- 598 *Dev.* **82**, 268-280. (doi:10.1002/mrd.22471)
- 599 18 Jiang Y, Peichel CL, Torrance L, Rizvi Z, Thompson S, Palivela VV, Pham H, Ling F, Bolnick DI.
600 2017 Sensory trait variation contributes to biased dispersal of threespine stickleback in flowing water. *J.*
601 *Evol. Biol.* **30**, 681-695. (doi:10.1111/jeb.13035)
- 602 19 Simon V, Hyacinthe C, Rétaux S. 2019 Breeding behavior in the blind Mexican cavefish and its river-
603 dwelling conspecific. *PLoS ONE.* **14**, e0212591. (doi:10.1371/journal.pone.0212591)
- 604 20 Ma ZQ, Herzog H, Jiang YG, Zhao YH, Zhang DY. 2020 Exquisite structure of the lateral line system
605 in eyeless cavefish *Sinocyclocheilus tianlinensis* contrast to eyed *Sinocyclocheilus macrophthalmus*
606 (Cypriniformes: Cyprinidae). *Integr. Zool.* **15**, 314-328. (doi:10.1111/1749-4877.12430)
- 607 21 Romero A, Zhao YH, Chen XY. 2009 The hypogean fishes of China. *Environ. Biol. Fishes.* **86**, 211-
608 278. (doi:10.1007/s10641-009-9441-3)
- 609 22 Zhao YH, Zhang CG. 2009 *Endemic fishes of Sinocyclocheilus (Cypriniformes: Cyprinidae) in China*
610 -- *Species diversity, cave adaptation, systematics and zoogeography*. Beijing: Science Press.
- 611 23 Webb JF, Northcutt RG. 1997 Morphology and distribution of pit organs and canal neuromasts in
612 non-teleost bony fishes. *Brain Behav. Evol.* **50**, 139-151. (doi:10.1159/000113328)
- 613 24 Powers AK, Berning DJ, Gross JB. 2020 Parallel evolution of regressive and constructive craniofacial
614 traits across distinct populations of *Astyanax mexicanus* cavefish. *J. Exp. Zool. B Mol. Dev. Evol.* **334**,
615 450-462. (doi:10.1002/jez.b.22932)
- 616 25 George PL, Borouchaki H. 1998 *Delaunay triangulation and meshing: application to finite elements*.
617 Paris: Hermès.
- 618 26 Aurenhammer F, Klein R, Lee D-T. 2012 *Voronoi diagrams and delaunay triangulations*. World
619 Scientific.
- 620 27 Lee DT, Schachter BJ. 1980 Two algorithms for constructing a delaunay triangulation. *Int. J. Parallel*
621 *Program.* **9**, 219-242. (doi:10.1007/BF00977785)
- 622 28 Palmer AR, Strobeck C, Chippindale AK. 1993 Bilateral variation and the evolutionary origin of
623 macroscopic asymmetries. *Genetica.* **89**, 201-218. (doi:10.1007/BF02424514)
- 624 29 Gorlewicz A, Krawczyk K, Szczepankiewicz AA, Trzaskoma P, Mülle C, Wilczynski GM. 2020
625 Colocalization colormap – an ImageJ Plugin for the quantification and visualization of colocalized
626 signals. *Neuroinformatics.* **18**, 661-664. (doi:10.1007/s12021-020-09465-9)
- 627 30 Zeitvogel F, Schmid G, Hao L, Ingino P, Obst M. 2016 ScatterJ: An ImageJ plugin for the evaluation
628 of analytical microscopy datasets. *J. Microsc.* **261**, 148-156. (doi:10.1111/jmi.12187)
- 629 31 Cordelières F, Bolte S. 2008 JACoP v2.0: improving the user experience with co-localization studies.
630 *ImageJ User & Developer Conference.* 174-181.
- 631 32 Wang YS, Wu QH, Hu MQ, Liu B, Chai ZY, Huang R, Wang Y, Xu HD, Zhou L, Zheng LH, *et al.*
632 2017 Ligand- and voltage-gated Ca²⁺ channels differentially regulate the mode of vesicular neuropeptide
633 release in mammalian sensory neurons. *Sci. Signal.* **10**, eaal1683. (doi:10.1126/scisignal.aal1683)
- 634 33 Bolte S, Cordelières FP. 2007 A guided tour into subcellular colocalization in light microscopy. *J.*
635 *Microsc.* **224**, 213-232. (doi:10.1111/j.1365-2818.2006.01706.x)
- 636 34 Dunn KW, Kamocka MM, McDonald JH. 2011 A practical guide to evaluating colocalization in
637 biological microscopy. *Am. J. Physiol. Cell Physiol.* **300**, C723-C742. (doi:10.1152/ajpcell.00462.2010)
- 638 35 Manders EM, Stap J, Brakenhoff GJ, van Driel R, Aten JA. 1992 Dynamics of three-dimensional
639 replication patterns during the S-phase, analysed by double labelling of DNA and confocal microscopy.
640 *J. Cell Sci.* **103**, 857-862. (doi:10.1242/jcs.103.3.857)
- 641 36 Zinchuk V, Grossenbacher Zinchuk O. 2009 Recent advances in quantitative colocalization analysis:

- 642 focus on neuroscience. *Prog. Histochem. Cytochem.* **44**, 125-172. (doi:10.1016/j.proghi.2009.03.001)
- 643 37 Huelsenbeck JP, Ronquist F, Nielsen R, Bollback JP. 2001 Bayesian inference of phylogeny and its
644 impact on evolutionary biology. *Science.* **294**, 2310-2314. (doi:10.1126/science.1065889)
- 645 38 Revell LJ. 2012 Phytools: an R package for phylogenetic comparative biology (and other things).
646 *Methods Ecol. Evol.* **3**, 217-223. (doi:10.1111/j.2041-210X.2011.00169.x)
- 647 39 Planidin NP, Reimchen TE. 2021 Ecological predictors of lateral line asymmetry in stickleback
648 (*Gasterosteus aculeatus*). *Evol. Ecol.* **35**, 609-629. (doi:10.1007/s10682-021-10117-w)
- 649 40 Sharma S, Coombs S, Patton P, de Perera TB. 2009 The function of wall-following behaviors in the
650 Mexican blind cavefish and a sighted relative, the Mexican tetra (*Astyanax*). *J. Comp. Physiol. A.* **195**,
651 225-240. (doi:10.1007/s00359-008-0400-9)
- 652 41 Patton P, Windsor S, Coombs S. 2010 Active wall following by Mexican blind cavefish (*Astyanax*
653 *mexicanus*). *J. Comp. Physiol. A.* **196**, 853-867. (doi:10.1007/s00359-010-0567-8)
- 654 42 Burt de Perera T, Braithwaite VA. 2005 Laterality in a non-visual sensory modality — the lateral line
655 of fish. *Curr. Biol.* **15**, 241-242. (doi:10.1016/j.cub.2005.03.035)
- 656 43 Jiang YG, Fu JC, Zhang DY, Zhao YH. 2016 Investigation on the lateral line systems of two cavefish:
657 *Sinocyclocheilus Macrophthalmus* and *S. Microphthalmus* (Cypriniformes: Cyprinidae). *J. Bionic Eng.*
658 **13**, 108-114. (doi:10.1016/S1672-6529(14)60164-5)
- 659 44 McGaugh SE, Weaver S, Gilbertson EN, Garrett B, Rudeen ML, Grieb S, Roberts J, Donny A,
660 Marchetto P, Gluesenkamp AG. 2020 Evidence for rapid phenotypic and behavioural shifts in a recently
661 established cavefish population. *Biol. J. Linn. Soc.* **129**, 143-161. (doi:10.1093/biolinnean/blz162)
- 662 45 Dezfuli BS, Magosso S, Simoni E, Hills K, Berti R. 2009 Ultrastructure and distribution of superficial
663 neuromasts of blind cavefish, *Phreatichthys andruzzii*, juveniles. *Microsc. Res. Tech.* **72**, 665-671.
664 (doi:10.1002/jemt.20714)
- 665 46 Powers AK, Kaplan SA, Boggs TE, Gross JB. 2018 Facial bone fragmentation in blind cavefish arises
666 through two unusual ossification processes. *Sci. Rep.* **8**, 7015. (doi:10.1038/s41598-018-25107-2)
- 667 47 Soares D, Niemiller ML. 2020 Variation in cephalic neuromasts surface and cave-dwelling fishes of
668 the family amblyopsidae (teleostei: percopsiformes). *J. Cave Karst Stud.* **82**, 198-209.
669 (doi:10.4311/2019LSC0115)
- 670 48 Trokovic N, Herczeg G, Ghani NIA, Shikano T, Merilä J. 2012 High levels of fluctuating asymmetry
671 in isolated stickleback populations. *BMC Evol. Biol.* **12**, 115. (doi:10.1186/1471-2148-12-115)
- 672 49 Soares D, Niemiller ML. 2020 Extreme Adaptation in Caves. *Anat. Rec.* **303**, 15-23.
673 (doi:10.1002/ar.24044)
- 674 50 Krishnan J, Rohner N. 2017 Cavefish and the basis for eye loss. *Philos. Trans. R. Soc. Lond., B. Biol.*
675 *Sci.* **372**, 20150487. (doi:10.1098/rstb.2015.0487)
- 676 51 Fernandes VFL, Macaspac C, Lu L, Yoshizawa M. 2018 Evolution of the developmental plasticity
677 and a coupling between left mechanosensory neuromasts and an adaptive foraging behavior. *Dev. Biol.*
678 **441**, 262-271. (doi:10.1016/j.ydbio.2018.05.012)
- 679 52 Coombs S, Janssen J, Webb JF. Year Diversity of lateral line systems: evolutionary and functional
680 considerations. In: J. Atema, R. R. Fay, A. N. Popper, W. N. Tavolga, editors. *Sensory Biology of Aquatic*
681 *Animals*; 1988; New York, NY: Springer New York; 1988. 553-593.
- 682 53 Montgomery JC, Coombs S, Baker CF. 2001 The mechanosensory lateral line system of the hypogean
683 form of *Astyanax Fasciatus*. *Environ. Biol. Fishes.* **62**, 87-96. (doi:10.1023/A:1011873111454)
- 684 54 Yamamoto Y, Byerly MS, Jackman WR, Jeffery WR. 2009 Pleiotropic functions of embryonic *sonic*
685 *hedgehog* expression link jaw and taste bud amplification with eye loss during cavefish evolution. *Dev.*

- 686 *Biol.* **330**, 200-211. (doi:10.1016/j.ydbio.2009.03.003)
- 687 55 Zhao YH, Zhang CG. 2006 Past research and future development on endemic Chinese cavefish of
688 the genus *Sinocyclocheilus* (Cypriniformes, Cyprinidae). *Acta Zootaxonomica Sinica.* **31**, 769-777.
- 689 56 He Y, Chen XY, Xiao TQ, Yang JX. 2013 Three-dimensional morphology of the *Sinocyclocheilus*
690 *hyalinus* (Cypriniformes : Cyprinidae) horn based on synchrotron X-ray microtomography. *Zool. Res.*
691 **34**, 128-134. (doi:10.11813/j.issn.0254-5853.2013.E4-5.E128)
- 692 57 Teyke T. 1990 Morphological differences in neuromasts of the blind cave fish *Astyanax hubbsi* and
693 the sighted river fish *Astyanax mexicanus*. *Brain Behav. Evol.* **35**, 23-30. (doi:10.1159/000115853)
- 694 58 Wark AR, Peichel CL. 2010 Lateral line diversity among ecologically divergent threespine
695 stickleback populations. *J. Exp. Biol.* **213**, 108-117. (doi:10.1242/jeb.031625)
- 696 59 Zhao YH, Watanabe K, Zhang CG. 2006 *Sinocyclocheilus donglanensis*, a new cavefish (Teleostei:
697 Cypriniformes) from Guangxi, China. *Ichthyol. Res.* **53**, 121-128. (doi:10.1007/s10228-005-0317-z)
- 698 60 Culver D, Pipan T. 2019 *The biology of caves and other subterranean habitats*.
- 699 61 Xiao H, Chen SY, Liu ZM, Zhang RD, Li WX, Zan RG, Zhang YP. 2005 Molecular phylogeny of
700 *Sinocyclocheilus* (Cypriniformes: Cyprinidae) inferred from mitochondrial DNA sequences. *Mol.*
701 *Phylogenet. Evol.* **36**, 67-77. (doi:10.1016/j.ympev.2004.12.007)
- 702 62 Li ZQ, Guo BC, Li JB, He SP, Chen YY. 2008 Bayesian mixed models and divergence time estimation
703 of Chinese cavefishes (Cyprinidae: *Sinocyclocheilus*). *Chinese Science Bulletin.* **53**, 2342-2352.
704 (doi:10.1007/s11434-008-0297-2)
- 705